Research Square

Preprints are preliminary reports that have not undergone peer review.
They should not be considered conclusive, used to inform clinical practice,
or referenced by the media as validated information.

Clinical and MRI Characteristics of Neuromyelitis Optica Spectrum Disorder: A Retrospective Analysis of 11 Cases

Kaixi XU[1]

Lianyungang Affiliated Hospital of Nanjing University of Chinese Medicine, Lianyungang Hospital of Jiangsu Provincial Hospital of Chinese Medicine

Chunwei WANG[2]

Lianyungang Affiliated Hospital of Nanjing University of Chinese Medicine, Lianyungang Hospital of Jiangsu Provincial Hospital of Chinese Medicine

Jin WANG

anicon@126.com

Lianyungang Affiliated Hospital of Nanjing University of Chinese Medicine, Lianyungang Hospital of Jiangsu Provincial Hospital of Chinese Medicine

Guangrong Bian

Lianyungang Affiliated Hospital of Nanjing University of Chinese Medicine, Lianyungang Hospital of Jiangsu Provincial Hospital of Chinese Medicine

---

Research Article

Keywords: neuromyelitis optica spectrum disorder, aquaporin-4 antibody, magnetic resonance imaging, optic neuritis, transverse myelitis, area postrema syndrome, arterial spin labeling

Posted Date: November 27th, 2026

DOI: https://doi.org/10.21203/rs.3.rs-11345671/v1

License: This work is licensed under a Creative Commons Attribution 4.0 International License.
Read Full License

Additional Declarations: No competing interests reported.

Abstract

Objective

To investigate the clinical, laboratory, and MRI characteristics of neuromyelitis optica spectrum disorder (NMOSD) among central nervous system inflammatory demyelinating diseases, and to improve early diagnosis and differential diagnosis while reducing misdiagnosis and missed diagnosis.

Methods

Eleven patients admitted to the Department of Neurology of Lianyungang Affiliated Hospital of Nanjing University of Chinese Medicine between January 2019 and August 2026 who fulfilled the 2015 International Diagnostic Criteria for NMOSD were retrospectively enrolled. There were 4 males and 7 females, aged 30–61 years, with a mean age of 38.08 ± 10.48 years. All patients underwent cervical and thoracic spinal MRI; some underwent orbital and cranial MRI, DWI, MRA, contrast-enhanced scanning, 3D-pcASL, and MRS. Clinical manifestations, AQP4-IgG status, cerebrospinal fluid (CSF) findings, MRI lesion location, signal characteristics, enhancement patterns, and ASL/MRS findings were analyzed.

Results

Initial symptoms included right limb numbness with blurred vision in 3 cases, limb numbness in 4 cases, limb weakness with hiccups after eating or drinking and blurred vision in 1 case, blurred vision with slurred speech in 1 case, recurrent nausea and vomiting in 1 case, and headache in 1 case. AQP4-IgG was positive in 8 cases, negative in 1 case, and untested in 2 cases; CSF protein was elevated in 3 cases. MRI findings were as follows. (1) Optic nerve/optic tract involvement in 4 cases (optic nerve in 3, optic tract in 1), all bilateral, with lesion length exceeding one-half of the total optic nerve length; 2 cases showed marked enhancement. (2) Spinal cord involvement in 9 cases: cervical cord in 4, thoracic cord in 1, and both cervical and thoracic cord in 4; lesions spanned more than 3 contiguous vertebral segments in 7 cases and fewer than 3 segments in 2 cases. Lesions were predominantly centered in the central gray matter, hypointense or isointense on T1WI and hyperintense on T2WI/T2FLAIR; mild enhancement was seen in 4 cases and no enhancement in 5 cases. (3) Cranial abnormalities in 6 cases: brainstem involvement in 5; periependymal lesions around the fourth ventricle/dorsal medulla in 3; periventricular lesions in 1; centrum semiovale/basal ganglia involvement in 1; bilateral cerebral and cerebellar white matter involvement in 1; and bilateral temporal lobe involvement in 2. One case showed involvement of the posterior limb of the internal capsule corticospinal tract, temporopontine tract, and hippocampal body of the temporal lobe, with a characteristic "figure-of-eight" sign on axial T2FLAIR and a "waterfall-like" pattern on coronal images; ASL demonstrated hyperperfusion in the bilateral thalamus and temporal lobe hippocampus, without hyperperfusion in the corticospinal tract or temporopontine tract. Contrast-enhanced imaging showed patchy heterogeneous enhancement in 2 cases and linear/pen-point-like leptomeningeal enhancement around the ependyma in 3 cases; 3D-T2FLAIR-CUBE displayed

these findings more clearly than 3D-T1FLAIR-CUBE and 3D-T1WI. DWI showed mildly high signal in only 1 case, with low signal in the remaining cases; MRS showed no abnormalities in NAA or Cho.

Conclusion

NMOSD predominantly affects young and middle-aged women and may present with optic neuritis, myelitis, area postrema syndrome, brainstem syndrome, diencephalic syndrome, or cerebral syndrome. When MRI demonstrates long-segment bilateral optic nerve/optic tract involvement, longitudinally extensive transverse myelitis (LETM), lesions in the dorsal medulla and around the fourth ventricle/periependymal region, a "figure-of-eight" sign and "waterfall-like" pattern of the corticospinal tract, and ASL hyperperfusion in the thalamus and temporal lobe hippocampus, NMOSD should be strongly suspected. Serum AQP4-IgG testing should be performed promptly to achieve early diagnosis and treatment.

Introduction

Central nervous system (CNS) inflammatory demyelinating diseases include clinically isolated syndrome (CIS), multiple sclerosis (MS), neuromyelitis optica spectrum disorder (NMOSD), myelin oligodendrocyte glycoprotein antibody-associated disease (MOGAD), and autoimmune glial fibrillary acidic protein astrocytopathy (GFAP-A) (1–3). NMOSD is an independent disease entity distinct from CIS, MS, and MOGAD. NMOSD is a rare autoimmune inflammatory CNS disease whose principal pathogenic antibody is immunoglobulin G targeting aquaporin-4 (AQP4-IgG) (4). AQP4 is a water channel protein located on astrocytic foot processes and plays a key role in maintaining the physiological function of the blood-brain barrier (BBB) and the ependymal system. Binding of anti-AQP4 antibodies to their target antigen triggers complement-mediated astrocyte injury, which subsequently leads to demyelination and neuronal damage (4). NMOSD predominantly involves CNS regions with high AQP4 expression, including the optic nerve, spinal cord, dorsal medulla, brainstem, and thalamus/hypothalamus (5–7). Insufficient clinical awareness of NMOSD readily leads to misdiagnosis and missed diagnosis (8–9), and the disease may cause blindness, paralysis, and even death (10–13). Moreover, many patients with NMOSD are misdiagnosed with MS, and treatment according to MS protocols may aggravate NMOSD, thereby increasing the severity and/or frequency of relapses and worsening disability (14–18). With the application of new techniques such as diffusion-weighted imaging (DWI), three-dimensional pseudo-continuous arterial spin labeling (3D-pcASL), 3D-T1WI, and T2FLAIR-CUBE contrast-enhanced imaging, the capacity for early diagnosis of NMOSD has improved substantially. In the present study, based on the 2015 International Consensus Diagnostic Criteria for NMOSD (19), we retrospectively analyzed the clinical data of 11 patients with NMOSD and explored their imaging characteristics, aiming to improve early recognition and diagnostic proficiency among clinicians at all levels, reduce misdiagnosis and missed diagnosis, and emphasize the importance of early diagnosis and treatment. Early diagnosis and active treatment are crucial for preventing relapse and reducing neurological damage, and are therefore of important clinical significance.

1 Materials and Methods

1.1 Study Subjects

This study was approved by the Ethics Committee of Lianyungang Affiliated Hospital of Nanjing University of Chinese Medicine (Approval No. 2025-XIS-063), and all subjects voluntarily consented to undergo the examinations. Patients hospitalized in the Department of Neurology of Lianyungang Affiliated Hospital of Nanjing University of Chinese Medicine between January 2019 and August 2026 who fulfilled the diagnostic criteria for NMOSD were retrospectively enrolled. Among the 11 patients, 4 were male and 7 were female, with an age at onset of 30–61 years and a mean age of 38.08 ± 10.48 years.

The diagnostic criteria used were those of the International Panel on Neuromyelitis Optica Diagnosis (2015) (19). (1) Diagnostic criteria for AQP4-IgG-positive NMOSD: at least one core clinical characteristic; AQP4-IgG positivity detected by a reliable method (cell-based assay [CBA] recommended); and exclusion of other diagnoses. (2) Diagnostic criteria for AQP4-IgG-negative or AQP4-IgG-unknown NMOSD: at least two core clinical characteristics occurring in one or more clinical attacks, with all of the following conditions fulfilled: at least one core clinical characteristic must be optic neuritis, acute longitudinally extensive transverse myelitis (LETM), or area postrema syndrome; dissemination in space, defined as two or more different core clinical characteristics; and fulfillment of additional MRI requirements. AQP4-IgG must be negative or untested by a reliable method, and other diagnoses must be excluded. (3) Core clinical characteristics: optic neuritis; acute myelitis; area postrema syndrome, defined as episodes of hiccups, nausea, or vomiting unexplained by other causes; acute brainstem syndrome; acute diencephalic syndrome, with NMOSD-characteristic diencephalic lesions on brain MRI; and cerebral syndrome with NMOSD-characteristic cerebral lesions. (4) Additional MRI requirements for AQP4-IgG-negative or unknown NMOSD: for acute optic neuritis, brain MRI must show one of the following: normal brain MRI or only nonspecific white matter lesions; or a long T2 signal or T1-enhanced signal of the optic nerve exceeding one-half of the optic nerve length, or involvement of the optic chiasm. For acute myelitis, a longitudinally extensive spinal cord lesion extending over more than 3 contiguous vertebral segments, or, in patients with a history of myelitis, corresponding spinal cord atrophy exceeding 3 contiguous vertebral segments. For area postrema syndrome, a dorsal medullary/area postrema lesion. For acute brainstem syndrome, a brainstem ependymal lesion.

Inclusion criteria: fulfillment of the 2015 International Diagnostic Criteria for Neuromyelitis Optica (19) and age ≥ 18 years. Exclusion criteria: presence of other CNS demyelinating diseases, including MS, MOGAD, or acute disseminated encephalomyelitis; diagnosis of any connective tissue disease (e.g., systemic lupus erythematosus, Sjögren syndrome, rheumatoid arthritis, vasculitis) or other autoimmune disease (e.g., autoimmune thyroid disease, myasthenia gravis) before the onset of NMOSD; pregnancy or lactation; concurrent severe chronic or acute disease (e.g., malignancy, severe hepatic or renal insufficiency, cardiovascular disease); and confirmed pre-existing severe psychiatric disorder, dementia, or cognitive/language impairment precluding communication.

1.2 Instruments and Methods

Among the 11 patients, orbital examination was performed in 5 cases with enhancement in 4; cervical and thoracic spinal examination in 11 cases with enhancement in 11; and cranial MR, DWI, and MRA in 11 cases with enhancement in 7. One patient underwent cranial conventional MRI, DWI, MRA, and 3D-ASL, and one patient underwent cranial conventional MRI, DWI, MRA, 3D-ASL, MRS, and contrast-enhanced examination.

A GE Discovery 750 3.0T scanner with an 8-channel phased-array body coil was used. Cervical and thoracic spinal MRI parameters were as follows. Cervical OSagT2FSE: TR 2500 ms, TE 125 ms, slice thickness 3 mm, echo train length 16, bandwidth 41.67 kHz, FOV 24 cm × 24 cm, matrix 224 × 320, NEX 2, flip angle 110°. OSangT1flair: TR 467 ms, TE 16.19 ms, slice thickness 3 mm, echo train length 4, bandwidth 31.25 kHz, FOV 24 cm × 24 cm, matrix 192 × 320, NEX 2, flip angle 110°. IDEAL: TR 2280 ms, TE 107.04 ms, slice thickness 3 mm, echo train length 16, bandwidth 83.35 kHz, FOV 24 cm × 24 cm, matrix 192 × 320, NEX 2, flip angle 110°. Thoracic OSagT2FSE: TR 2500 ms, TE 125.63 ms, slice thickness 4 mm, echo train length 21, bandwidth 62.5 kHz, FOV 34 cm × 34 cm, matrix 256 × 320, NEX 4, flip angle 142°. OSangT1flair: TR 458 ms, TE 11.76 ms, slice thickness 4 mm, echo train length 4, bandwidth 62.5 kHz, FOV 34 cm × 34 cm, matrix 256 × 320, NEX 2, flip angle 110°. IDEAL: TR 2000 ms, TE 101.84 ms, slice thickness 4 mm, echo train length 4, bandwidth 83.35 kHz, FOV 34 cm × 34 cm, matrix 192 × 320, NEX 2, flip angle 110°. OSang/OCorT1 + C: TR 540 ms, TE 8.54 ms, slice thickness 4 mm, echo train length 3, bandwidth 50 kHz, FOV 34 cm × 34 cm, matrix 256 × 320, NEX 2, flip angle 110°.

A 32-channel phased-array dedicated head coil was used for orbital and cranial examinations. Orbital examination: T1WI sequence TR 713.00 ms, TE 9.20 ms, acquisition time 0:56 min; T2WI TR 3559 ms, TE 82.18 ms, acquisition time 1:57 min; coronal T2WI TR 7000 ms, TE 74.54 ms, acquisition time 3:58 min; sagittal T2WI TR 2500 ms, TE 90.07 ms, acquisition time 2:25 min; contrast-enhanced axial T1WI TR 713.00 ms, TE 9.20 ms, acquisition time 0:56 min; sagittal TR 453.00 ms, TE 9.14 ms, acquisition time 1:24 min; coronal TR 721.00 ms, TE 9.31 ms, acquisition time 1:39 min; field of view (FOV) 20 cm × 20 cm, slice thickness 3.0 mm, flip angle 111°, bandwidth 244.14 kHz, matrix 320 × 192. Cranial examination sequences: unenhanced T1WI, T2WI, T2FLAIR, DWI, and ADC, and post-contrast T1FLAIR, 3D OAx Bravo, T2FLAIR, and 3D-Sag Cube T2FLAIR. T1WI sequence: TR 1827.06 ms, TE 20.54 ms, acquisition time 0:54 min; T2WI: TR 5689 ms, TE 101.82 ms; T2FLAIR: TR 8500 ms, TE 146.29 ms; FOV 24 cm × 24 cm, slice thickness 5.0 mm, flip angle 12°, bandwidth 83.33 kHz, matrix 256 × 256, acquisition time 2:43 min. 3D OAx Bravo parameters: TR 8.21 ms, TE 3.22 ms, FOV 24 cm × 24 cm, slice thickness 1.0 mm, flip angle 12°, bandwidth 31.25 kHz, matrix 256 × 256, acquisition time 3:30 min. 3D Cube T2FLAIR parameters: sagittal acquisition, TR 5000 ms, TE 129.58 ms, FOV 25.6 cm × 25.6 cm, slice thickness 1.0 mm, echo train length 1, bandwidth 31.25 kHz, matrix 256 × 256, acquisition time 6:53 min. 3D-PCASL parameters: TR/TE = 5327 ms/10.54 ms, FOV 24 cm × 24 cm, matrix 1024 × 8, slice thickness 4 mm, interslice gap 1.5 mm, number of acquisitions 1, number of excitations 3, acquisition time 2 min 25 s. MRS was acquired using multi-voxel spectroscopy: TR/TE 1000/144 ms, matrix 18 × 18, FOV 24 cm × 24 cm, slice thickness 10 mm, gap 0 mm, number of excitations (NEX) 1, bandwidth 2 kHz, flip angle

90°. The contrast agent Gd-DTPA was manually injected via the antecubital vein at a dose of 0.1 mmol/kg.

1.3 Image Processing and Interpretation

Raw MRS and 3D-PCASL data were transferred to a GE Advantage Workstation 4.6, and MRS processing software was applied. 3D-PCASL perfusion analysis software was used to obtain data and calculate CBF maps. Color images were automatically generated, ranging from red to dark blue, with red representing high perfusion and blue representing low perfusion. Regions of interest were manually outlined at the same slice, same location, same region, and same mirror region as the largest lesion on DWI, avoiding the ventricles as much as possible, to obtain the 3D-PCASL quantitative parameter—regional cerebral blood flow (rCBF)—and to observe changes in rCBF in and around the lesion.

Image interpretation: images were jointly analyzed by two physicians, and the final results were reviewed and confirmed by an associate chief physician and a chief physician (with 20 years of MRI diagnostic experience).

2 Results

2.1 Clinical Characteristics

Initial symptoms were right limb numbness with blurred vision in 3 cases, limb numbness in 4 cases, limb weakness with hiccups after eating or drinking and blurred vision in 1 case, blurred vision with slurred speech in 1 case, recurrent nausea and vomiting in 1 case, and headache in 1 case (Table 1).

2.2 Auxiliary Examinations

Serum AQP4-IgG was detected using a cell-based assay (CBA) kit. CSF examination: lumbar puncture was performed; CSF was colorless and transparent with normal pressure; CSF protein was elevated in 3 cases. AQP4-IgG was positive in 8 cases, negative in 1 case, and untested in 2 cases.

2.3 Imaging Characteristics

MRI findings in the 11 patients (Table 1) were as follows. (1) Optic nerve lesions: 3 cases showed optic nerve involvement and 1 case showed optic tract swelling, with increased signal on T2WI or T2FLAIR; all cases showed bilateral optic nerve/optic tract involvement, and lesion length exceeded one-half of the total optic nerve length; 2 cases showed marked enhancement on contrast-enhanced scanning (Fig. 1a-c, 3n). (2) Spinal cord lesions: 9 cases showed abnormal spinal cord signal, all involving the cervical and/or thoracic cord, including cervical cord in 4 cases, thoracic cord in 1 case, and both cervical and thoracic cord in 4 cases; lesions spanned more than 3 contiguous vertebral segments in 7 cases and fewer than 3 contiguous vertebral segments in 2 cases. MRI showed spinal cord swelling with a central distribution, predominantly involving the central gray matter; isointense or hypointense on T1WI (Fig. 2j) and hyperintense on T2WI or T2FLAIR (Fig. 2k); 4 cases showed mild enhancement (Fig. 1i) and 5 cases showed no enhancement. (3) Cranial lesions: 6 cases showed abnormal cranial signal, involving the

brainstem, thalamus, lateral ventricle, external capsule, periventricular region of the fourth ventricle, and cerebral hemisphere white matter. Brainstem involvement was present in 5 cases (Fig. 1d, 2f, 2g, 3a-i); periependymal lesions around the ventricular system were present in 4 cases, including dorsal brainstem lesions adjacent to the fourth ventricle in 3 cases (Fig. 1d, 1k, 2d, 2h, 2i, 3h) and periependymal lesions surrounding the lateral ventricle in 1 case (Figs. 2a-c, 2e); involvement of the centrum semiovale and basal ganglia in 1 case (Fig. 1e, 1g, 1h, 1j); and involvement of bilateral cerebral and cerebellar white matter in 1 case. One case involved the corticospinal tract in the posterior limb of the internal capsule, the temporopontine tract, and the hippocampal body of the temporal lobe, and ASL showed hyperperfusion in the bilateral thalamus and temporal lobe hippocampus, with no hyperperfusion in the corticospinal tract or temporopontine tract (Fig. 3j-m); bilateral temporal lobe involvement was present in 2 cases (Fig. 3l). Most lesions were patchy or plaque-like, clearly visualized as high signal on T2WI and T2FLAIR, with some lesions showing low or isointense signal on T1WI (Fig. 1d, 1e, 1h, 1j, 2b, 2d, 2f, 3b, 3j, 3l, 3n). DWI showed mildly high signal in only 1 case (Fig. 2c) and low signal in the remaining cases (Fig. 3c). Bilateral involvement of the corticospinal tract in the posterior limb of the internal capsule and the temporopontine tract was roughly symmetric, presenting a "figure-of-eight" sign (Fig. 3j), with a bilateral "waterfall-like" pattern on coronal images (Fig. 3n); no enhancement was observed; MRS showed no abnormalities in N-acetylaspartate (NAA) or choline (Cho) (Fig. 3q). On contrast-enhanced examination, 2 cases showed patchy heterogeneous enhancement (Fig. 3d-h), and 3 cases showed linear (Fig. 1k, 2h-i, 3g-h) or pen-point-like (Fig. 2e) leptomeningeal enhancement around the ependyma; contrast-enhanced 3D-T2FLAIR-CUBE (Fig. 2i, 3h) displayed these findings more clearly than contrast-enhanced 3D-T1FLAIR-CUBE (Fig. 2h, 3g) and 3D-T1WI. After treatment, lesions were largely absorbed (Fig. 3i), reduced in size (1h), or recurred (Fig. 1i, 2f-g, 3j-l).

3 Discussion

3.1 Clinical Features and Pathology

NMOSD is a rare, highly relapsing autoimmune disease of the CNS characterized predominantly by inflammatory attacks involving the optic nerves, spinal cord, and brain, and often resulting in severe neurological disability. Its core pathogenic mechanism involves pathogenic autoantibodies targeting AQP4-IgG on astrocytic foot processes; after high-affinity binding to the antigen, the antibody activates the complement cascade and promotes the release of pro-inflammatory cytokines such as interleukin-6, thereby disrupting the blood-brain barrier and causing astrocyte injury and dysfunction, ultimately leading to demyelination and neurological deficits (20–23). In addition, NMOSD may overlap with other systemic autoimmune diseases, and such comorbidities may increase the annualized relapse rate and affect prognosis (25–26).

The global prevalence of NMOSD is approximately 0.5–10 per 100,000 population, with significant geographic and ethnic differences (27). The age-standardized prevalence in Asia is approximately 3.0 per 100,000, higher than that in Caucasian populations (approximately 1.0 per 100,000) (28). In 2020, China published data from a hospital-based registry (2016–2018) of inpatients with NMOSD, showing an

incidence of approximately 0.278 per 100,000 person-years (29). The disease can occur at any age (4–88 years), but the peak onset is usually in early adulthood (median age 32–41 years) (12, 30). Among AQP4-IgG-positive patients, the female-to-male ratio can reach (8–9):1 (31), while among seronegative patients the female-to-male ratio reaches 3:1 (15, 30). Although NMOSD can occur at any age, its peak onset in early adulthood—a period critical for career development, family responsibilities, and social participation—makes its impact particularly profound (32).

In the present cohort of 11 patients, there were 4 males and 7 females, with a male-to-female ratio of approximately 1.75:1; age at onset ranged from 30 to 61 years, with a mean age of 38.08 ± 10.48 years; disease duration ranged from 10 months to 9 years, with 2–6 attacks; serum AQP4-IgG was positive in 8 cases, negative in 1 case, and untested in 2 cases. The slight female predominance and predominantly young-to-middle-aged onset in this cohort are broadly consistent with the overall characteristics of NMOSD; however, the male-to-female ratio was lower than that reported in classic studies (8–9):1, which may be related to the single-center design, small sample size, and retrospective selection bias. Initial symptoms were predominantly limb numbness/weakness, blurred vision, hiccups after eating or drinking, recurrent nausea and vomiting, and headache, consistent with the six core clinical syndromes of NMOSD.

NMOSD is characterized by a high relapse rate and a heavy disability burden. Although biologics have significantly reduced the annualized relapse rate, each acute attack may still cause stepwise cumulative neurological damage (11). In the absence of adequate treatment, many patients rapidly develop permanent functional impairment, including severe vision loss, restricted mobility, chronic neuropathic pain, and sphincter dysfunction (13). Within 5 years of onset, approximately 50% of patients require wheelchair assistance and 30% become functionally blind (6). NMOSD has six core clinical syndromes, including optic neuritis, acute myelitis, area postrema syndrome, acute brainstem syndrome, acute diencephalic syndrome, and cerebral syndrome (19), each with corresponding characteristic imaging findings.

3.2 Optic Neuritis: Clinical and MRI Features

Optic neuritis (ON) presents clinically with blurred vision, decreased visual acuity, headache, retrobulbar pain, and dyschromatopsia; involvement of the optic chiasm may cause bitemporal visual field defects with non-central scotomas, and severe cases may experience severe vision loss. MRI shows linear or plaque-like high signal on T2 or T2FLAIR, with possible enhancement on post-gadolinium T1-weighted imaging. Features suggesting NMOSD include longitudinally extensive optic nerve lesions extending to the optic chiasm or even the optic tract, as well as simultaneous or sequential bilateral involvement; nearly 50% of cases have bilateral optic nerve involvement (33). The extent of involvement often exceeds one-half of the total optic nerve length, and in the acute phase, contrast-enhanced scanning may show marked enhancement of the optic nerve and its sheath (34–35). In the present cohort, 3 cases had optic nerve involvement and 1 case had optic tract swelling; all showed bilateral optic nerve/optic tract involvement, with high signal on T2WI or T2FLAIR and lesion length exceeding one-half of the total optic

nerve length; 2 cases showed marked enhancement on contrast-enhanced scanning. These findings are consistent with the longitudinally extensive and bilateral features of NMOSD-related optic neuritis.

3.3 Myelitis: Clinical and MRI Features

Myelitis often presents with sensory, motor (including respiratory), and bladder/bowel dysfunction. LETM on MRI is an important imaging manifestation of acute myelitis in NMOSD, involving the spinal cord over more than 3 contiguous vertebral segments. LETM is present in 85% of cases, whereas approximately 15% present with short-segment transverse myelitis (STM) (36–38). The most common locations are the cervical region and the upper-to-middle thoracic region (39). Spinal cord lesions appear hyperintense on T2WI and T2-FLAIR, predominantly involving the central gray matter of the cervical and upper thoracic cord; in most cases, the spinal cord is markedly swollen in the acute phase, and enhancement may be seen on post-gadolinium T1-weighted sequences. In more than 40% of patients, lesions are markedly hyperintense on T2-weighted imaging, and so-called "bright spotty lesions" may be seen (40–41), resulting in alternating areas of high and relatively low signal on T2 images. Although the spinal cord is swollen, these bright areas usually do not show gadolinium (Gd) enhancement. Axial MRI may show a butterfly or H-shaped pattern, which is relatively specific. Recurrent attacks may lead to spinal cord atrophy, manifested as focal or diffuse T2WI hyperintensity in the involved segments, with absent or weak enhancement. STM lesions located centrally in the spinal cord with low signal on T1 should raise suspicion for NMO and warrant AQP4-Ab testing. STM is common during the first episode of myelitis, and in more than 90% of patients, lesions recur and become LETM. Lesions are often centrally located, involve the gray matter, and favor the cervical or upper thoracic cord, and may extend upward to the lower brainstem; this pattern suggests NMOSD. Extensive spinal cord atrophy suggests previous NMOSD attacks. Extensive lesions, marked edema, persistent gadolinium enhancement, and the presence of T1 hypointensity are associated with a poor prognosis. In the present cohort, 9 cases showed abnormal spinal cord signal, with cervical cord involvement in 4 cases, thoracic cord in 1 case, and both cervical and thoracic cord in 4 cases; lesions involved more than 3 contiguous vertebral segments in 7 cases and fewer than 3 contiguous vertebral segments in 2 cases. MRI showed spinal cord swelling with predominantly central gray matter involvement, isointense or hypointense signal on T1WI and hyperintense signal on T2WI/T2FLAIR; 4 cases showed mild enhancement and 5 cases showed no enhancement. These results further support that LETM and central gray matter involvement are important imaging features of NMOSD-related myelitis; however, short-segment lesions may also be observed, requiring comprehensive assessment in combination with clinical findings and antibody testing.

3.4 Clinical and Imaging Features of Brain Lesions

Brain parenchymal involvement is relatively common in NMOSD, with an abnormal brain MRI rate of approximately 50%–80% (42–43). Lesions predominantly occur in regions with high AQP4 expression, such as the dorsal medulla, brainstem tegmentum, periependymal region of the fourth ventricle, diencephalon, and deep cerebral white matter, consistent with the corresponding clinical symptoms. In initial cases, approximately 20%–40% show no abnormalities or only minimal nonspecific changes (44–

45). The value of brain MRI for accurate diagnosis of NMOSD and its differentiation from multiple sclerosis (MS) has received increasing attention (46–47). Previous multicenter analyses found that 29%–42.5% of patients with NMOSD were misdiagnosed with MS, delaying the diagnosis of NMOSD and the initiation of subsequent preventive immunotherapy (14). It is well known that many MS treatments may aggravate NMOSD, thereby increasing the severity and/or frequency of relapses and worsening disability (17, 48). Fortunately, diagnostic delay has decreased substantially in recent years, mainly owing to the specificity of the AQP4 antibody biomarker (49).

Area postrema syndrome (APS) is the third most common manifestation of NMOSD, affecting approximately 30% of patients, and may occur at onset or during the disease course (50). APS involves the dorsal area postrema of the medulla; the area postrema is the chemoreceptor trigger zone, and once inflammation involves the vagal control of vomiting and hiccups, it manifests as intractable hiccups and nausea/vomiting. These symptoms may occur simultaneously or in isolation, may have an acute onset or a chronic course, and usually persist for more than 72 hours; because of their severity and associated weight loss, they are often misdiagnosed as digestive system diseases and lead to hospitalization (51). APS lesions involve the dorsal area postrema of the medulla. Because brain parenchymal lesions mainly occur in regions with high AQP4 expression, they appear as linear or band-like high signal on T2WI, T2-FLAIR, or 3D-T2FLAIR-CUBE; they generally show no or inconspicuous enhancement on conventional T1-enhanced imaging, whereas linear leptomeningeal enhancement may be seen on 3D-T1FLAIR-CUBE or 3D-T2FLAIR-CUBE, with 3D-T2FLAIR-CUBE showing more pronounced enhancement than 3D-T1FLAIR-CUBE. Lesions often extend downward to connect with upper cervical spinal cord lesions; they may also involve the pons, brachium pontis, cerebellar peduncle, and floor of the fourth ventricle. Linear medullary lesions are a characteristic manifestation of NMO brainstem lesions and are often bilateral on sagittal images; when lesions extend downward and form a continuous lesion with the cervical spinal cord, this has certain diagnostic implications (52–54). If MRI shows an area postrema lesion, APS can be diagnosed when nausea, vomiting, and/or hiccups persist for less than 48 hours.

Acute brainstem syndrome often presents with headache, diplopia, facial palsy, ataxia, and vestibular or brainstem cranial nerve nuclear/fascicular involvement, and may also be asymptomatic. Acute diencephalic syndrome manifests as sleep disturbance, eating disorders, or thermoregulatory dysfunction, as well as hyponatremia associated with syndrome of inappropriate antidiuretic hormone secretion (SIADH). Lesions of acute diencephalic and brainstem syndromes are mainly distributed in the third ventricle, the diencephalon around the midbrain aqueduct, the ependymal region of the anterior midbrain, the brainstem tegmentum, the region around the fourth ventricle and ependyma, and the cerebellopontine angle. Lesions in the thalamus and hypothalamus appear as diffuse, patchy T2 or T2FLAIR hyperintensity with indistinct margins; contrast-enhanced 3D-T1FLAIR-CUBE or 3D-T2FLAIR-CUBE often shows linear enhancement of ependymal lesions, whereas diencephalic and brainstem lesions show mild patchy enhancement or no enhancement.

Acute cerebral syndrome lesions mainly involve the corpus callosum, periependymal region of the lateral ventricle, cerebral hemisphere white matter, and corticospinal tract. Among these, deep cerebral

hemispheric white matter lesions are often large and confluent, mimicking tumors; disruption of the astrocytic membrane leads to "cloud-like" enhancement of the lesions, and ependymal injury leads to periependymal enhancement, which are relatively characteristic imaging findings of NMOSD (5, 55–56). Corpus callosum involvement occurs in 12%–18% of NMOSD cases; in the acute phase, the corpus callosum shows multiple, large confluent lesions with heterogeneous signal, hypointense margins and hyperintense centers on T2WI, surrounding edema, and a "marbled" appearance on T2FLAIR, involving half of the total length of the corpus callosum; when the full thickness of the corpus callosum is extensively involved, an "arch bridge-like" appearance is seen (55, 57). In the chronic phase, the corpus callosum becomes atrophic and cystic, and lesions decrease, with reduced signal or even disappearance. Corticospinal tract lesions: corticospinal tract lesions are continuous lesions extending longitudinally along the pyramidal tract; that is, lesions may extend from the posterior limb of the internal capsule to the base of the pons, with indistinct margins distributed along the pyramidal tract, with an incidence of 23%–44% (56), and may be unilateral or bilateral. In unilateral involvement, coronal T2FLAIR may show lesions extending from the posterior limb of the internal capsule to the pontine peduncle, with indistinct margins and high signal distributed along the pyramidal tract; corticospinal tract lesions resemble a flowing waterfall, and extensive involvement of the midbrain-diencephalic junction resembles a waterfall pool. In the present cohort, 6 cases (54.5%) had abnormal brain MRI findings, including brainstem involvement in 5 cases; periependymal lesions around the ventricular system in 4 cases, including dorsal brainstem/dorsal medullary lesions adjacent to the fourth ventricle in 3 cases and periventricular ependymal lesions around the lateral ventricle in 1 case; involvement of the centrum semiovale/basal ganglia in 1 case; bilateral cerebral and cerebellar white matter involvement in 1 case; and bilateral temporal lobe involvement in 2 cases. One case showed involvement of the corticospinal tract in the posterior limb of the internal capsule, the temporopontine tract, and the hippocampal body of the temporal lobe, with a typical "figure-of-eight" sign on axial T2FLAIR and a typical "waterfall-like" pattern on coronal T2FLAIR; ASL showed symmetric hyperperfusion in the bilateral thalamus and temporal lobe hippocampus, whereas no hyperperfusion was observed in the corticospinal tract or temporopontine tract. Most lesions showed no or mild enhancement on contrast-enhanced scanning; 2 cases showed patchy heterogeneous enhancement, and 3 cases showed linear or pen-point-like leptomeningeal enhancement around the ependyma; 3D-T2FLAIR-CUBE displayed leptomeningeal/ependymal enhancement more clearly than 3D-T1FLAIR-CUBE and 3D-T1WI. DWI showed mildly high signal in only 1 case and low signal in the remaining cases; MRS showed no abnormalities in NAA or Cho. These findings are consistent with the distribution of regions with high AQP4 expression, suggesting that the dorsal medulla, the region around the fourth ventricle, the periependymal region around the lateral ventricle, and the corticospinal tract should be carefully evaluated, and that combined 3D-T2FLAIR-CUBE enhancement is recommended to improve lesion detection.

4 Differential Diagnosis

NMOSD should be mainly differentiated from MS and MOGAD.

The age at onset of NMOSD is approximately 40 years, with a female-to-male ratio of 8–9:1, and there are six clinical manifestations. Optic nerve lesion length often exceeds one-half of the optic nerve, and the posterior optic nerve or optic chiasm may be involved. Spinal cord involvement is prominently longitudinally extensive (≥ 3 vertebral segments), although short-segment involvement may occur early and become longitudinally extensive after recurrent attacks. Lesions involve the central portion of the spinal cord and radiate toward the ependymal surface, with a typical "H" sign and bright spotty enhancement. Brain involvement often presents as linear T2FLAIR hyperintensity in the area postrema, floor of the fourth ventricle, periaqueductal gray matter, hypothalamus, and third ventricular wall, with "cloud-like" enhancement in the brain parenchyma, diffuse corpus callosum involvement with a "marbled" or "arch bridge-like" appearance, and a "waterfall-like" or "diversion waterfall-like" pattern of the corticospinal tract; MRS shows no abnormalities in NAA or Cho. CSF and serum AQP4-IgG are often positive.

The age at onset of MS is approximately 30 years, with a female-to-male ratio of 3:1. Clinical manifestations commonly include optic neuritis, partial myelitis, and brainstem and cerebellar symptoms; optic nerve and spinal cord lesions are short-segmented and involve the periphery of the spinal cord, predominantly the posterior and lateral columns, with less frequent involvement of the central gray matter. MS lesions are predominantly distributed in the supratentorial cerebral hemispheric white matter and show dissemination in space and time, mainly involving periventricular white matter, focal and inferior portions of the corpus callosum, and subcortical white matter. Lesions are round or ovoid, some showing a "perpendicular sign," with a "black hole" appearance on T1WI, a "fried egg" appearance on T2WI, and a "central vein sign" on SWI; acute-phase contrast enhancement may be ring-like or open-ring-like, MRS shows decreased NAA and increased Cho, and the corticospinal tract is rarely involved (60).

MOGAD is more common in children than in adults, with a female-to-male ratio of 1–2:1. Optic neuritis is the most common initial phenotype, bilateral in approximately 50% of cases, with long segments involving the anterior optic nerve, generally without optic chiasm involvement, and with widening around the optic nerve sheath. The next most common presentation is myelitis, which is usually longitudinally extensive but may be short-segmented, and more readily extends to the lumbar cord. Acute disseminated encephalomyelitis (ADEM), brainstem or cerebellar features, or cerebral cortical encephalitis may occur (61). Serum MOG-IgG is positive.

In the present cohort, AQP4-IgG was positive in 8 cases, negative in 1 case, and untested in 2 cases; for seronegative or untested patients, NMOSD cannot be excluded solely on the basis of a negative antibody result, and the core clinical features and additional MRI requirements in the 2015 diagnostic criteria should be combined, with differentiation from MS and MOGAD. The imaging findings in this cohort were characterized by long-segment optic nerve/optic tract involvement, LETM, dorsal medullary and periependymal lesions around the fourth ventricle, the "figure-of-eight" sign of the corticospinal tract, and ASL hyperperfusion in the thalamus and temporal lobe hippocampus, which differ from the typical MS

findings of supratentorial periventricular ovoid lesions, short-segment peripheral spinal cord lesions, and open-ring enhancement.

5 Limitations

This study was a single-center retrospective study with a sample size of only 11 cases, including 1 AQP4-IgG-negative and 2 untested cases; no pathological or genetic verification was performed, and follow-up durations varied, so selection bias may exist. Future studies should expand the sample size, standardize MRI scanning protocols, and conduct long-term follow-up for validation.

6 Conclusion

In summary, NMOSD is a severe autoimmune disease of the CNS characterized by recurrent attacks that can lead to significant sequelae, particularly visual and motor impairment. It predominantly affects young and middle-aged women and may present with six core clinical features, with certain characteristic MRI findings. The results of the present cohort suggest that when MRI shows long-segment bilateral optic nerve/optic tract involvement, long-segment transverse myelitis, cranial lesions involving the dorsal medulla, diencephalon, or ependymal/periependymal parenchyma with linear T2FLAIR hyperintensity, a "figure-of-eight" sign and "waterfall-like" pattern of the corticospinal tract, and ASL hyperperfusion in the thalamus and temporal lobe hippocampus, NMOSD should be strongly suspected, and serum AQP4-IgG testing should be recommended. Early diagnosis, timely intervention, and improvement of prognosis are of critical importance.

Declarations

Funding: Key Project of the Lianyungang Science and Technology Key R&D Program (Social Development) (SF2323) and Key Project of Lianyungang Traditional Chinese Medicine Technology Development Plan (grant numbers: ZD202207).

Credit Author Statement

Kaixi Xu and Chunwei WANG are co-first authors.Kaixi Xu Chunwei WANG and Guangrong Bian: data collection. Guangrong Bian and Jin WANG: data analysis. Kaixi Xu and Jin WANG: experimental design. All authors read and approved the final manuscript.

Acknowledgments

We would like to express our sincere gratitude to Professor Kaixi Xu and Professor Jin WANG for he key suggestions on the study design and in-depth guidance on data interpretation.

Data Availability Statement

The datasets generated and/or analyzed during the current study are not publicly available due to hospital policies and patient confidentiality restrictions but are available from the corresponding author on reasonable request.

Conflict of Interest Statement: The authors declare that there are no conflicts of interest.

Ethics Approval and Consent to Participate

This study was approved by the Ethics Committee of Lianyungang Affiliated Hospital of Nanjing University of Chinese Medicine (Approval No. 2025-XIS-063). The authors confirm that all procedures involving human participants were performed in accordance with the ethical standards of the institutional and/or national research committee and with the 1964 Helsinki Declaration and its later amendments or comparable ethical standards, and with relevant guidelines and regulations. All subjects voluntarily consented to undergo the examinations. The requirement for written informed consent was waived by the committee due to the retrospective nature of the study. Because all images and data were anonymized, separate patient consent for publication was not required, as confirmed by the ethics committee. All authors approved the final manuscript and consented to publication.

Consent for Publication Not applicable. All data and images are presented in anonymized form and contain no identifiable patient information. The Ethics Committee of Lianyungang Affiliated Hospital of Nanjing University of Chinese Medicine waived the requirement for separate written informed consent for publication owing to the retrospective nature of the study and the use of anonymized data (Approval No. 2025-XIS-063).

Statement: All data and images are presented in anonymized form. No identifiable patient information is included.

References

1. Al-Ani A, Chen JJ, Costello F. Myelin oligodendrocyte glycoprotein antibody-associated disease (MOGAD): current understanding and challenges[J]. J Neurol. 2023,270(8):4132-4150. doi: 10.1007/s00415-023-11737-8.
2. Tang CL, Fok EWS. Low-Positive Myelin Oligodendrocyte Glycoprotein (MOG)-Immunoglobulin G (IgG) in Pediatric Demyelinating Disease: How Imaging Features Can Support a MOG Antibody-Associated Disease (MOGAD) Diagnosis[J]. Cureus. 2026,18(5):e109271. doi: 10.7759/cureus.109271.
3. Zhang M, Han J, Xia J, et al. Chinese neuroimmunological disease (NIDBase) cohort study: cohort profile[J]. BMJ Open. 2026,16(1):e099386. doi: 10.1136/bmjopen-2025-099386.
4. Bonan L, Camilli F, Bombardi M, et al. The cascade sign in aquaporin-4-IgG positive (AQP4-IgG+) NMOSD[J]. Mult Scler. 2025,31(14):1679-1682. doi: 10.1177/13524585251356820.

5. Chien C, Cruz E Silva V, Geiter E, et al; Guthy-Jackson Charitable Foundation International Clinical Consortium for NMOSD. Aquaporin-4 Immunoglobulin G-seropositive Neuromyelitis Optica Spectrum Disorder MRI Characteristics: Data Analysis from the International Real-World PAMRINO Study Cohort[J]. Radiology. 2024,313(2):e233099. doi: 10.1148/radiol.233099.
6. Neuroimmunology Group of the Society of Neurology, Chinese Medical Association. Chinese guidelines for the diagnosis and treatment of neuromyelitis optica spectrum disorders (2025 edition)[J]. Chinese Journal of Neurology. 2025,58(7):687-703. DOI:10.3760/cma.j.cn113694-20250211-00075.
7. Committee on Neuroimmunology and Related Diseases, Beijing Neuroscience Society. Expert consensus on biological targeted therapy for neuromyelitis optica spectrum disorders in China (2026 edition)[J]. Chin J Neuroimmunol Neurol. 2026,33(3):313-321. doi:10.3969/j.issn.1006-2963.2026.03.001.
8. Min JH, Waters P, Vincent A, et al. Symptomatic brain involvement as the initial manifestation of neuromyelitis optica[J]. J Clin Neurosci, 2013,20(7):938-942. DOI:10.1016/j.jocn.2012.08.007.
9. Szewczyk AK, Papuć E, Mitosek-Szewczyk K, et al. NMOSD-Diagnostic Dilemmas Leading towards Final Diagnosis[J]. Brain Sci. 2022,12(7):885. doi: 10.3390/brainsci12070885.
10. Bilodeau PA, Wruble Clark M, Ganguly A, et al. Real-World Efficacy and Safety of Neuromyelitis Optica Spectrum Disorder Disease-Modifying Treatments[J]. Neurol Neuroimmunol Neuroinflamm. 2026,13(2):e200536. doi: 10.1212/NXI.0000000000200536.
11. Pittock SJ, Barnett M, Bennett JL, et al. Ravulizumab in Aquaporin-4-Positive Neuromyelitis Optica Spectrum Disorder[J]. Ann Neurol. 2023,93(6):1053-1068. doi: 10.1002/ana.26626.
12. Lei ZY, Li HP, Yang Q, et al. Quality of life and its influencing factors in patients with neuromyelitis optica spectrum disorder[J]. Front Neurol. 2026,17:1797747. doi: 10.3389/fneur.2026.1797747.
13. Meca-Lallana JE, Gómez-Ballesteros R, Pérez-Miralles F, et al. Impact of Neuromyelitis Optica Spectrum Disorder on Quality of Life from the Patients' Perspective: An Observational Cross-Sectional Study[J]. Neurol Ther. 2022,11(3):1101-1116. doi: 10.1007/s40120-022-00356-6.
14. Mealy MA, Wingerchuk DM, Greenberg BM, et al. Epidemiology of neuromyelitis optica in the United States: a multicenter analysis[J]. Arch Neurol. 2012,69(9):1176-1180. doi: 10.1001/archneurol.2012.314.
15. Jarius S, Ruprecht K, Wildemann B, et al. Contrasting disease patterns in seropositive and seronegative neuromyelitis optica: A multicentre study of 175 patients[J]. J Neuroinflammation. 2012,9:14. doi: 10.1186/1742-2094-9-14.
16. Carnero Contentti E, Delgado-García G, Criniti J, et al. An Abnormally High Neutrophil-to-Lymphocyte Ratio Is Not an Independent Outcome Predictor in AQP4-IgG-Positive NMOSD[J]. Front Immunol. 2021,12:628024. doi: 10.3389/fimmu.2021.628024.
17. Yamout BI, Beaini S, Zeineddine MM, et al. Catastrophic relapses following initiation of dimethyl fumarate in two patients with neuromyelitis optica spectrum disorder[J]. Mult Scler. 2017,23(9):1297-1300. doi: 10.1177/1352458517694086.

18. Zabad RK, Stewart R, Healey KM. Pattern Recognition of the Multiple Sclerosis Syndrome[J]. Brain Sci. 2017,7(10):138. doi: 10.3390/brainsci7100138.
19. Wingerchuk DM, Banwell B, Bennett JL, et al. International consensus diagnostic criteria for neuromyelitis optica spectrum disorders[J]. Neurology, 2015,85(2):177-189. DOI: 10.1212/wnl.0000000000001729.
20. Pittock SJ, Zekeridou A, Weinshenker BG. Hope for patients with neuromyelitis optica spectrum disorders - from mechanisms to trials[J]. Nat Rev Neurol. 2021,17(12):759-773. doi: 10.1038/s41582-021-00568-8.
21. Lucchinetti CF, Guo Y, Popescu BF, et al. The pathology of an autoimmune astrocytopathy: lessons learned from neuromyelitis optica[J]. Brain Pathol. 2014,24(1):83-97. doi: 10.1111/bpa.12099.
22. Richard C, Ruiz A, Cavagna S, et al. Connexins in neuromyelitis optica: a link between astrocytopathy and demyelination[J]. Brain. 2020,143(9):2721-2732. doi: 10.1093/brain/awaa227.
23. Shi S, Liu Y, Fu Z, et al. Comparison of clinical and laboratory characteristics of neuromyelitis optica spectrum disorder with or without anti-connective tissue antibodies: an 18-month cohort follow-up[J]. Front Immunol. 2026,17:1829927. doi: 10.3389/fimmu.2026.1829927.
24. Wang Z, Wu L, Zhang Z, et al. Overlap syndrome of anti-aquaporin-4 positive neuromyelitis optica spectrum disorder and mixed connective tissue disease: a case report[J]. Front Immunol. 2025,16:1644259. doi: 10.3389/fimmu.2025.1644259.
25. Samadzadeh S, Chan F, Francis A, et al. The impact of autoimmune comorbidities on the onset attack recovery in adults with AQP4-NMOSD and MOGAD[J]. J Neurol. 2025,272(7):453. doi: 10.1007/s00415-025-13180-3.
26. Chan F, Berhanu D, Samadzadeh S, et al. Smoking status and vascular risk factors as predictors of disability in AQP4-NMOSD and MOGAD[J]. Mult Scler. 2025,31(6):658-667. doi: 10.1177/13524585251325069.
27. Papp V, Magyari M, Aktas O, et al. Worldwide Incidence and Prevalence of Neuromyelitis Optica: A Systematic Review[J]. Neurology. 2021,96(2):59-77. doi: 10.1212/WNL.0000000000011153.
28. Hor JY, Asgari N, Nakashima I, et al. Epidemiology of Neuromyelitis Optica Spectrum Disorder and Its Prevalence and Incidence Worldwide[J]. Front Neurol. 2020,11:501. doi: 10.3389/fneur.2020.00501.
29. Tian DC, Li Z, Yuan M, et al. Incidence of neuromyelitis optica spectrum disorder (NMOSD) in China: a national population-based study[J]. Lancet Reg Health West Pac, 2020,2:100021. DOI: 10.1016/j.lanwpc.2020.100021.
30. Clarke L, Arnett S, Lilley K, et al. Magnetic resonance imaging in neuromyelitis optica spectrum disorder[J]. Clin Exp Immunol. 2021,206(3):251-265. doi: 10.1111/cei.13630.
31. Borisow N, Kleiter I, Gahlen A, et al. Influence of female sex and fertile age on neuromyelitis optica spectrum disorders[J]. Mult Scler, 2017,23(8):1092-1103. DOI:10.1177/1352458516671203.
32. Fandit L, Asgari N, Apiwattanakul M, et al; GJCF International Clinical Consortium & Biorepository for Neuromyelitis Optica. Demographic and clinical features of neuromyelitis optica: A review[J]. Mult

Scler. 2015,21(7):845-853. doi: 10.1177/1352458515572406.

33. Carnero Contentti E, Delgado-García G, López PA, et al. Acute optic nerve lesions in first-ever NMOSD-related optic neuritis using conventional brain MRI: A Latin American multicenter study[J]. Mult Scler Relat Disord. 2020,46:102558. doi: 10.1016/j.msard.2020.102558.
34. Dutra BG, da Rocha AJ, Nunes RH, Maia ACM Júnior. Neuromyelitis Optica Spectrum Disorders: Spectrum of MR Imaging Findings and Their Differential Diagnosis[J]. Radiographics. 2018,38(1):169-193. doi: 10.1148/rg.2018170141.
35. Jarius S, Aktas O, Ayzenberg I, et al; Neuromyelitis Optica Study Group (NEMOS). Update on the diagnosis and treatment of neuromyelitis optica spectrum disorders (NMOSD) - revised recommendations of the Neuromyelitis Optica Study Group (NEMOS). Part I: Diagnosis and differential diagnosis[J]. J Neurol. 2023,270(7):3341-3368. doi: 10.1007/s00415-023-11634-0.
36. Pekmezovic T, Mesaros S, Momcilovic N, et al. Nationwide epidemiological study of neuromyelitis optica spectrum disorder in Serbia[J]. Mult Scler Relat Disord. 2025,102:106708. doi: 10.1016/j.msard.2025.106708.
37. Cai W, Tan S, Zhang L, et al. Linear lesions may assist early diagnosis of neuromyelitis optica and longitudinally extensive transverse myelitis, two subtypes of NMOSD[J]. J Neurol Sci. 2016,360:88-93. doi: 10.1016/j.jns.2015.11.040.
38. Singh N, Bhatia R, Bali P, et al. Clinical Features, Gender Differences, Disease Course, and Outcome in Neuromyelitis Optica Spectrum Disorder[J]. Ann Indian Acad Neurol. 2021,24(2):186-191. doi: 10.4103/aian.AIAN_334_20.
39. Bigaut K, Lambert C, Kremer L, et al. Atypical myelitis in patients with multiple sclerosis: Characterization and comparison with typical multiple sclerosis and neuromyelitis optica spectrum disorders[J]. Mult Scler. 2021,27(2):232-238. doi: 10.1177/1352458520906995.
40. Salama S, Levy M. Bright spotty lesions as an imaging marker for neuromyelitis optica spectrum disorder[J]. Mult Scler. 2022,28(11):1663-1666. doi: 10.1177/1352458521994259.
41. Rabasté S, Cobo-Calvo A, Nistiriuc-Muntean V, et al; OFSEP, NOMADMUS Study Group. Diagnostic value of bright spotty lesions on MRI after a first episode of acute myelopathy[J]. J Neuroradiol. 2021,48(1):28-36. doi: 10.1016/j.neurad.2020.04.006.
42. Mir TA, Hassan T, Ahmad SH, et al. Clinicoradiologic profile of neuromyelitis optica spectrum disorder in a Kashmiri cohort: a prospective observational cohort study[J]. Encephalitis. 2026,6(3):65-74. doi: 10.47936/encephalitis.2025.00164.
43. Sato D, Fujihara K. Atypical presentations of neuromyelitis optica[J]. Arq Neuropsiquiatr. 2011,69(5):824-828. doi: 10.1590/s0004-282x2011000600019.
44. Abdullah S, Fadzli F, Ramli N, et al. There is less MRI brain lesions and no characteristic MRI Brain findings in IIDDs patients with positive AQP4 serology among Malaysians[J]. Mult Scler Relat Disord. 2017,12:34-38. doi: 10.1016/j.msard.2016.12.011.
45. Cao G, Duan Y, Zhang N, et al. Brain MRI characteristics in neuromyelitis optica spectrum disorders: A large multi-center retrospective study in China[J]. Mult Scler Relat Disord. 2020,46:102475. doi:

10.1016/j.msard.2020.102475.

46. Huh SY, Min JH, Kim W, et al. The usefulness of brain MRI at onset in the differentiation of multiple sclerosis and seropositive neuromyelitis optica spectrum disorders[J]. Mult Scler. 2014,20(6):695-704. doi: 10.1177/1352458513506953.
47. Ghazanfari Hashemi M, Talebi V, Abbasi Kasbi N, et al. T1 hypointense brain lesions in NMOSD and its relevance with disability: a single institution cross-sectional study[J]. BMC Neurol. 2024,24(1):62-68. doi: 10.1186/s12883-024-03550-1.
48. Furlan R, Schaedelin S, Frederiksen JL, et al. Granulocyte and astrocyte markers distinguish MOG-antibody disease and neuromyelitis optica from multiple sclerosis[J]. Brain. 2026,149(4):1319-1331. doi: 10.1093/brain/awaf345.
49. Mealy MA, Mossburg SE, Kim SH, et al. Long-term disability in neuromyelitis optica spectrum disorder with a history of myelitis is associated with age at onset, delay in diagnosis/preventive treatment, MRI lesion length and presence of symptomatic brain lesions[J]. Mult Scler Relat Disord. 2019,28:64-68. doi: 10.1016/j.msard.2018.12.011.
50. Khalilidehkordi E, Clarke L, Arnett S, et al. Relapse Patterns in NMOSD: Evidence for Earlier Occurrence of Optic Neuritis and Possible Seasonal Variation[J]. Front Neurol. 2020,11:537. doi: 10.3389/fneur.2020.00537.
51. Popescu BF, Lennon VA, Parisi JE, et al. Neuromyelitis optica unique area postrema lesions: nausea, vomiting, and pathogenic implications[J]. Neurology, 2011,76(14):1229-1237. DOI: 10.1212/WNL.0b013e318214332c.
52. Kim SH, Hyun JW, Joung A, et al. Occurrence of asymptomatic acute neuromyelitis optica spectrum disorder-typical brain lesions during an attack of optic neuritis or myelitis[J]. PLOS ONE. 2016,11(12):e0167783. doi: 10.1371/journal.pone.0167783.
53. Asgari N, Skejoe HP, Lillevang ST, et al. Modifications of longitudinally extensive transverse myelitis and brainstem lesions in the course of neuromyelitis optica (NMO): a population-based, descriptive study[J]. BMC Neurol. 2013,13:33. doi: 10.1186/1471-2377-13-33.
54. Kim W, Lee JE, Kim SH, et al. Cerebral Cortex Involvement in Neuromyelitis Optica Spectrum Disorder[J]. J Clin Neurol. 2016,12(2):188-193. doi: 10.3988/jcn.2016.12.2.188.
55. Kim HJ, Paul F, Lana-Peixoto MA, et al; Guthy-Jackson Charitable Foundation NMO International Clinical Consortium & Biorepository. MRI characteristics of neuromyelitis optica spectrum disorder: an international update[J]. Neurology. 2015,84(11):1165-1173. doi: 10.1212/WNL.0000000000001367.
56. Costello F. Neuromyelitis Optica Spectrum Disorders[J]. Continuum (Minneap Minn). 2022,28(4):1131-1170. doi: 10.1212/CON.0000000000001168.
57. Kim W, Park MS, Lee SH, et al. Characteristic brain magnetic resonance imaging abnormalities in central nervous system aquaporin-4 autoimmunity[J]. Mult Scler. 2010,16(10):1229-1236. doi: 10.1177/1352458510376640.

58. Carnero Contentti E, Lopez PA, Tkachuk V, et al. Frequency of new asymptomatic MRI lesions during attacks and follow-up of patients with NMOSD in a real-world setting[J]. Mult Scler. 2023,29(10):1240-1249. doi: 10.1177/13524585231187120.
59. Camera V, Holm-Mercer L, Ali AAH, et al. Frequency of New Silent MRI Lesions in Myelin Oligodendrocyte Glycoprotein Antibody Disease and Aquaporin-4 Antibody Neuromyelitis Optica Spectrum Disorder[J]. JAMA Netw Open. 2021,4(12):e2137833. doi: 10.1001/jamanetworkopen.2021.37833.
60. Ma YN, Wang Q, Ma SR, et al. Differential diagnosis between NMOSD and MS: a retrospective study based on clinical and imaging features[J]. Front Neurol. 2026,17:1718736. doi: 10.3389/fneur.2026.1718736.
61. Banwell B, Bennett JL, Marignier R, et al. Diagnosis of myelin oligodendrocyte glycoprotein antibody-associated disease: international MOGAD panel proposed criteria[J]. Lancet Neurol. 2023,22(2):268-282. doi: 10.1016/S1474-4422(22)00431-8.

Table 1

Table 1 Clinical manifestations, laboratory findings, and MRI lesion locations in 11 patients with NMOSD

Case	Sex	Age	Initial clinical symptom	Disease duration	Number of attacks	AQP4	MRI lesion location and enhancement
1	Male	30	Blurred vision	7 y 3 mo	6	Positive	Bilateral optic nerves, external capsule, centrum semiovale, pons, left insula, around the fourth ventricle, right anterior horn of the lateral ventricle, and left insula, with recurrent involvement. C5-7 and T10-L1 spinal cord swelling with linear high-signal enhancement
2	Female	49	Left limb weakness, hiccups after eating or drinking, blurred vision, slurred speech	10 mo	3	Positive	Bilateral temporal lobe hippocampus, right temporal lobe and posterior horn of the lateral ventricle with patchy enhancement, C1-2 spinal cord linear enhancement
3	Female	35	Right limb numbness	13 mo	2	Untested	C4-7 lesions, with patchy enhancement at C5-6
4	Female	34	Headache	2 y	2	Positive	Roundish lesion in the medulla oblongata with ring enhancement
5	Male	30	Limb numbness	2 y 10 mo	3	Negative	Medulla oblongata, C1-7, extensive cerebral and cerebellar lesions; no thoracic cord enhancement
6	Female	61	Right lower limb weakness and blurred vision	9 y	5	Positive	T4-8, bilateral optic nerve high signal, no enhancement
7	Female	56	Bilateral lower limb weakness	3 y 10 mo	4	Untested	C5-7, T1-5, T2-3 linear enhancement, spinal cord atrophy, bilateral optic nerve thickening
8	Male	33	Right limb numbness	1 y	2	Positive	C1-T3 mild enhancement

Case	Sex	Age	Initial clinical symptom	Disease duration	Number of attacks	AQP4	MRI lesion location and enhancement
9	Female	32	Bilateral lower limb weakness	2 y 4 mo	2	Positive	C6-T4, no enhancement
10	Male	37	Recurrent nausea and vomiting	2 y 7 mo	6	Positive	Adjacent to the right posterior horn of the lateral ventricle, ventral medulla, and fourth ventricle with linear enhancement; enlargement of the C6-7 spinal cord lesion with central canal dilatation and enhancement
11	Female	30	Left blurred vision	2 y 1 mo	5	Positive	Pons and right brachium pontis, fourth ventricle with punctate and linear enhancement; on follow-up, lesions appeared in the corticospinal tract with no enhancement; ASL showed hyperperfusion around the lesion; bilateral optic tracts showed high signal on FLAIR

Figures

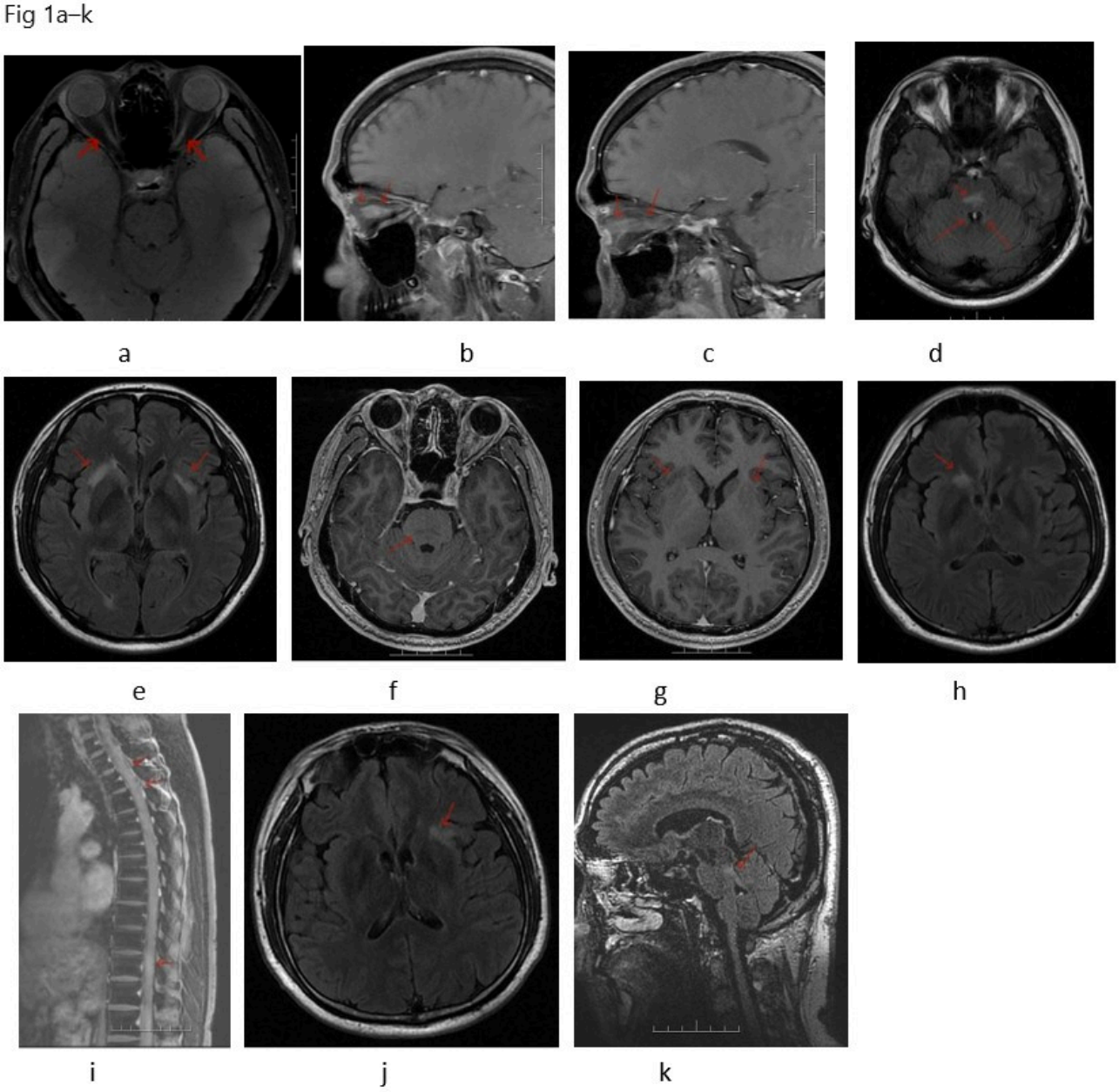

Figure 1

a–k: Patient A. The patient presented with blurred vision at initial presentation. a) Axial orbital T1WI. b–c) Sagittal contrast-enhanced T1WI of the right and left orbits, showing diffuse swelling of the bilateral optic nerves with marked enhancement. d–f) Axial T2FLAIR images show linear and patchy hyperintensities in the pons (short red arrow), around the ependyma of the fourth ventricle (long red arrow), adjacent to the anterior horn of the right lateral ventricle, and in the bilateral external capsules (arrows). f–g) Axial contrast-enhanced T1WI shows no enhancement. h) T2FLAIR image at follow-up after treatment shows a small patchy lesion adjacent to the anterior horn of the right lateral ventricle, with disappearance of the bilateral thalamic lesions. i) Simultaneous sagittal contrast-enhanced thoracolumbar MRI shows swelling of the C5–7 and T10–L1 spinal cord with linear enhancing high signal. j) T2FLAIR image at subsequent follow-up shows a new lesion in the left external capsule (red

arrow). k) Contrast-enhanced T2FLAIR-CUBE at later follow-up shows linear leptomeningeal enhancement around the tectum of the midbrain and the fourth ventricle (red arrow).

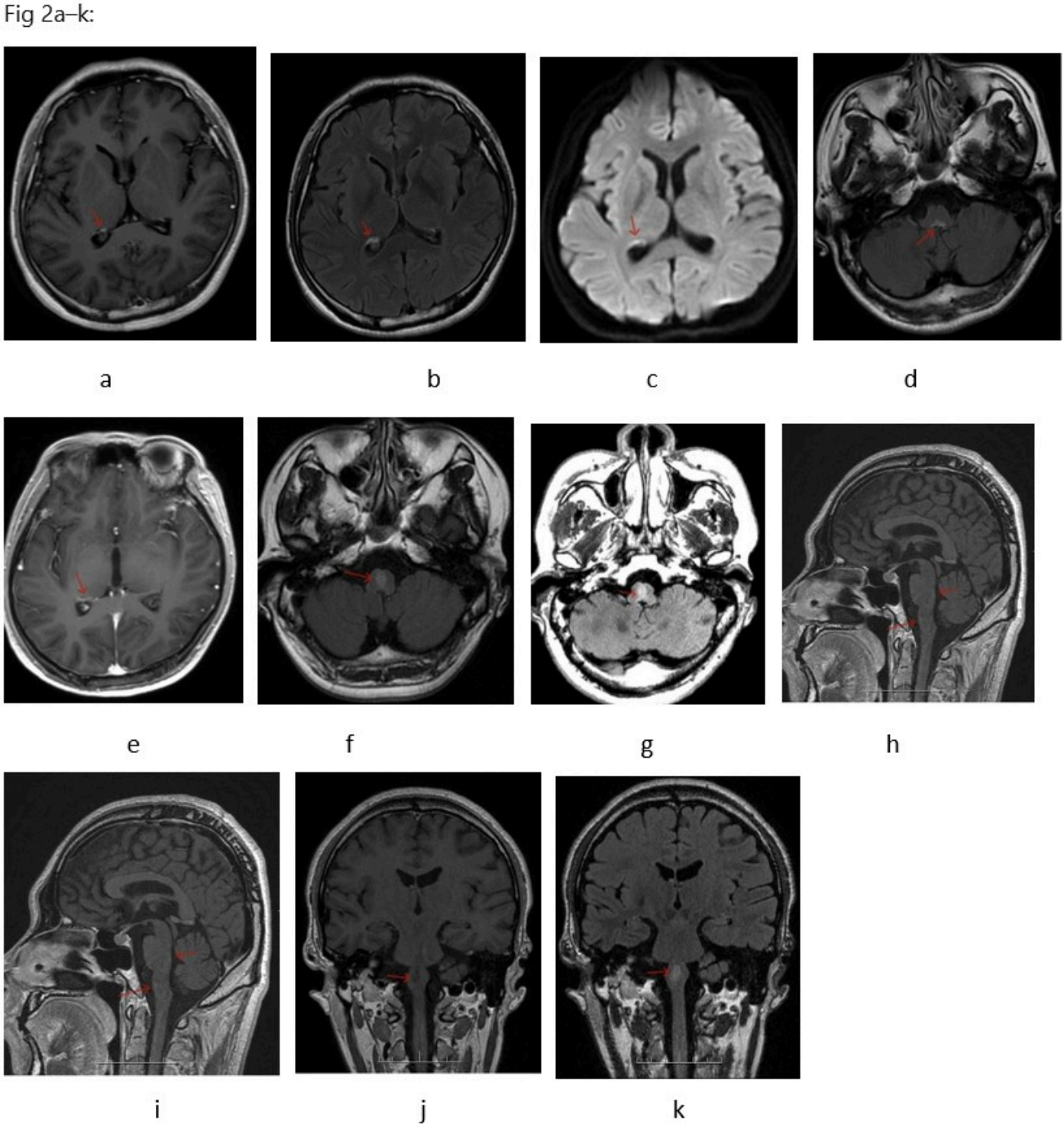

Figure 2

a–k: Patient B. The patient presented with recurrent nausea. At initial presentation, the patient had recurrent nausea; during follow-up, the patient was admitted with worsening recurrent nausea and vomiting; later, the patient was admitted again with dizziness and diplopia, with recurrence. a) T1WI

shows a linear slightly hyperintense lesion adjacent to the posterior horn of the right lateral ventricle; b) T2FLAIR and c) DWI show a long linear hyperintense lesion; d) T2FLAIR shows a hyperintense lesion around the ependyma of the fourth ventricle (red arrow). e) Contrast-enhanced T1WI shows pen-point-like enhancement adjacent to the posterior horn of the right lateral ventricle. At later follow-up, dizziness with diplopia for 5 months, recurrence for 3 days. f) T2FLAIR and g) 3D-T2FLAIR-CUBE show a new patchy hyperintense lesion in the medulla oblongata (red arrow). h) 3D-T1WI-CUBE and i) 3D-T2FLAIR-CUBE sagittal contrast-enhanced images show linear leptomeningeal enhancement anterior to the fourth ventricle and medulla oblongata (red arrow); 3D-T2FLAIR-CUBE (i) shows leptomeningeal enhancement more clearly than 3D-T1WI-CUBE (h). j) 3D-T1WI-CUBE and k) 3D-T2FLAIR-CUBE coronal images show involvement of the central gray matter in the medulla oblongata with spinal cord swelling (red arrow).

Fig 3a–n.

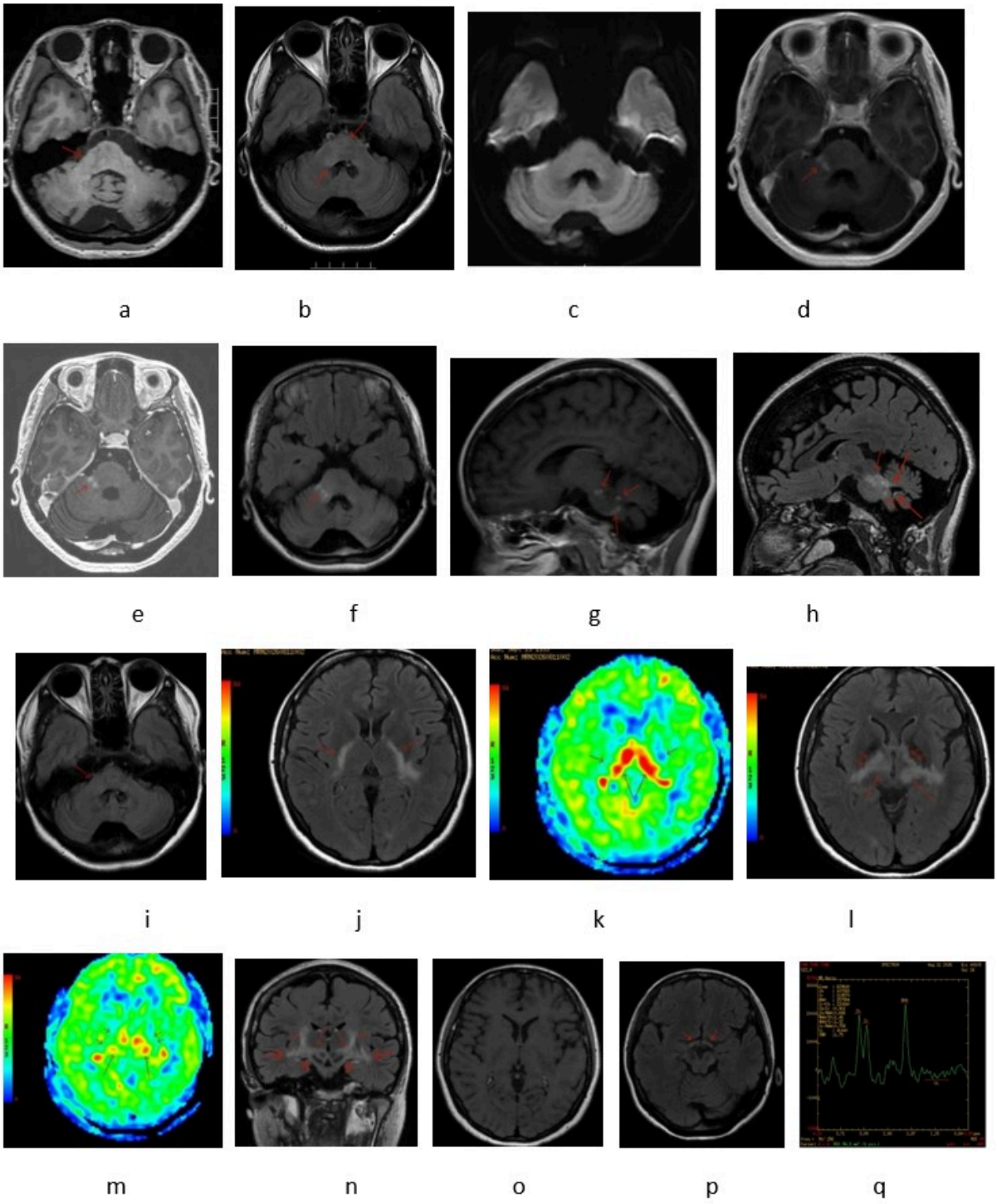

Figure 3

a–q: Patient C. The patient presented with blurred vision in the left eye at presentation. a) T1WI and b) T2FLAIR show small patchy long T1 and long T2 signal lesions in the pons and right brachium pontis (red arrows). c) DWI shows no high signal. d) T1WI, e) 3D-OAx T1 BRAVO, and f) contrast-enhanced 3D-OAx T2FLAIR-CUBE show scattered patchy enhancing lesions in the right brachium pontis (red arrows). g) Contrast-enhanced 3D-sagittal T1-CUBE and h) 3D-sagittal T2-CUBE show patchy enhancement in the

pons (short red arrow); h also shows leptomeningeal enhancement at the fourth ventricle (long red arrow). i) Follow-up T2FLAIR at later follow-up shows disappearance of the pontine lesion. At subsequent follow-up, the patient's blurred vision worsened. j–m) 3D-ASL shows typical "figure-of-eight" hyperintense signal of the bilateral corticospinal tracts within the posterior limbs of the internal capsules (short red arrows in j and l on T2FLAIR), and linear/patchy hyperintense lesions in the bilateral thalami (long red arrows in l on T2FLAIR); ASL images show no hyperperfusion in the bilateral corticospinal tracts (short red arrows) or temporopontine tracts, and symmetric hyperperfusion in the bilateral thalami (long red arrows in k and l). n) Coronal 3D-T2FLAIR-CUBE shows linear/patchy hyperintense signal in the bilateral corticospinal tracts (short thin red arrows), bilateral thalami (long thin red arrows), bilateral hippocampal bodies of the temporal lobe limbic system (long thick red arrows), and bilateral temporopontine tracts (short thick red arrows), representing a typical "diversion waterfall-like" pattern. o) Contrast-enhanced T1WI shows no enhancement of the corticospinal tracts. p) T2FLAIR shows linear hyperintense signal in the bilateral optic tracts (red arrows). q) MRS shows no abnormalities in N-acetylaspartate (NAA) or choline (Cho).